Electronic Supplementary Material (ESI) for Journal of Materials Chemistry A.

Supporting Information for:

Investigating Two-Step $MAPbI_3$ Thin Film Formation during Spin Coating by Simultaneous in Situ Absorption and Photoluminescence Spectroscopy

Mihirsinh Chauhan,[1,2,#] Yu Zhong,[1,3,#] Konstantin Schötz,[1] Brijesh Tripathi,[2] Anna Köhler,[1,4] Sven Huettner[3], Fabian Panzer[1*]

1: Soft Matter Optoelectronics, University of Bayreuth, 95440 Bayreuth, Germany

2: School of Technology, Pandit Deendayal Petroleum University, 382007 Gandhinagar, India

3: Department of Chemistry, University of Bayreuth, 95440 Bayreuth, Germany

4: Bayreuth Institute of Macromolecular Research (BIMF) and Bavarian Polymer Institute (BPI), University of Bayreuth, 95440 Bayreuth, Germany.

#: Authors contributed equally

Corresponding Author: fabian.panzer@uni-bayreuth.de

S1: Additional OD and PL spectra

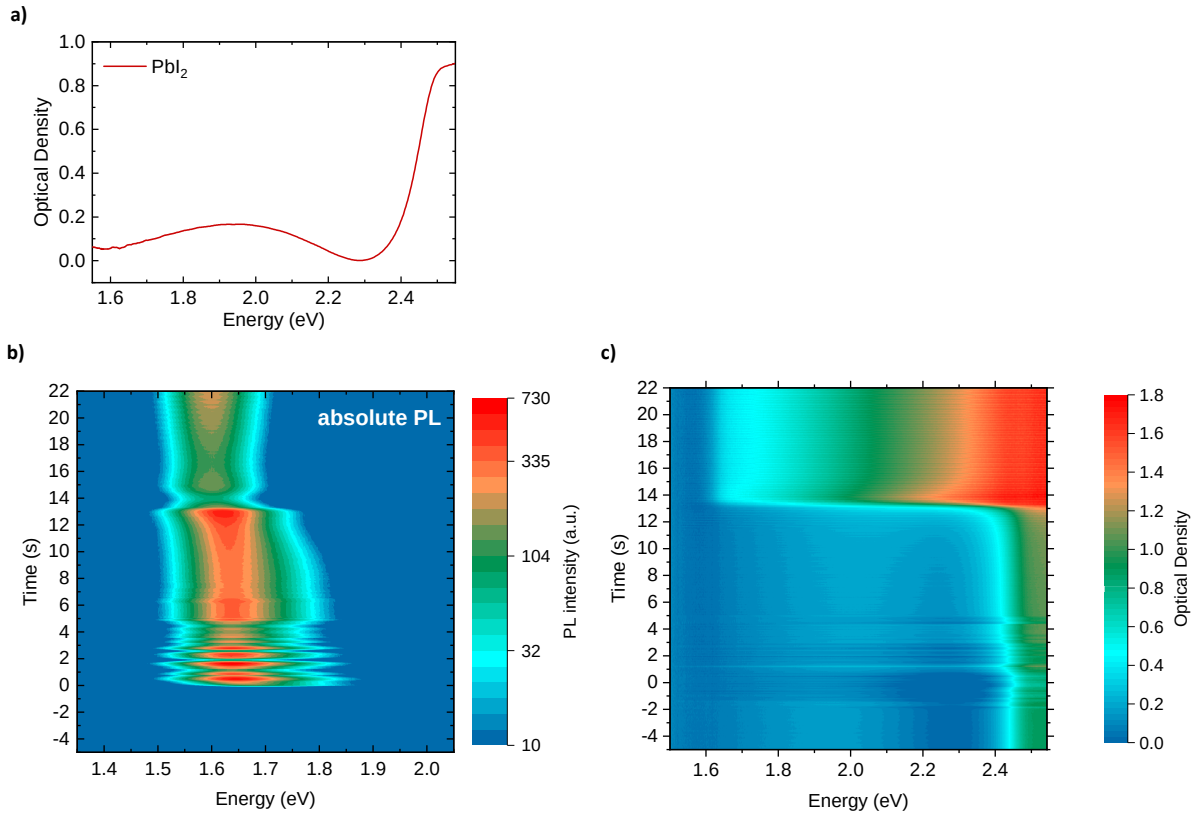

Figure S1: (a) Optical Density of the neat PbI_2 layer. (b) 2D map of the temporal evolution of the PL spectrum with absolute measured intensities as indicated with colors. (c) 2D map of the temporal evolution of the measured Optical Density with intensities as indicated with colors. As a reference spectrum I_0, the transmission through a blank quartz substrate was used.

S2: Fitting of hyperbolic secant to measured PL in range I

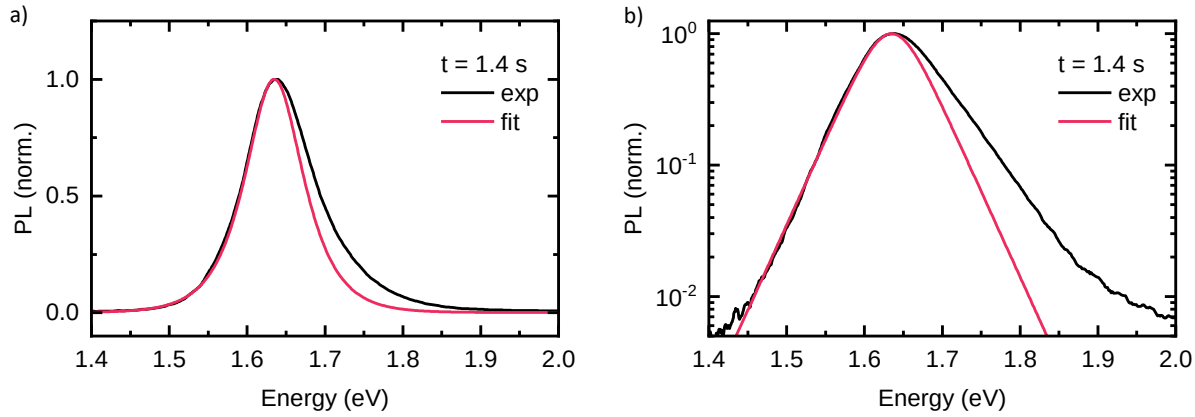

Figure S2: Normalized PL at t = 1.4 s (black) and a fit using a hyperbolic secant, demonstrating the asymmetry of the measured PL line shape, plotted on a (a) linear intensity scale and (b) log intensity scale.

S3: Calculation of $MAPbI_3$ crystal size from the PL spectra in range I using confinement approach:

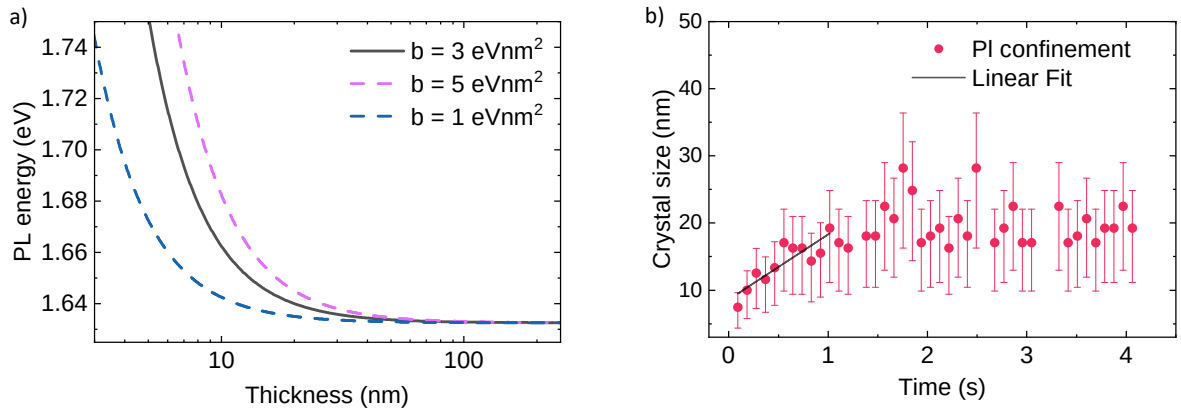

Figure S3: (a) Correlation between PL Peak energy E and crystal size d as proposed by Parrot et al.,[1] $E = E_g + \frac{b}{d^2}$ with E_g=1.63 eV and different b values of 1 eVnm^2 (dashed blue), 3 eVnm^2 (solid black) and 5 eVnm^2 (dashed purple). The curves for b=1 eVnm^2 and b=5 eVnm^2 were used to calculate the crystal size error. (b) Evolution of crystal size (red dots) within the first 4 seconds of processing, where the crystal size is calculated on the basis of the black line in (a). The initial growth rate was quantified using a linear fit in the time range up to 1.0 s (black line) where a slope of 11±2 nm/s is obtained.

S4: Extracted absorption edge of PL in range III

The optical density of the absorption edge was extracted by $OD = -\log\left(\frac{PL_{final}}{PL_{initial}}\right)$, where $PL_{initial}$ is the PL at $t = 9.1\ s$ and PL_{final} is the PL at $t = 12.6\ s$ scaled to the red falling edge of $PL_{initial}$. Note that this scaling procedure does not alter the spectral shape of the obtained absorption, but only shifts it up in OD to avoid negative ODs.

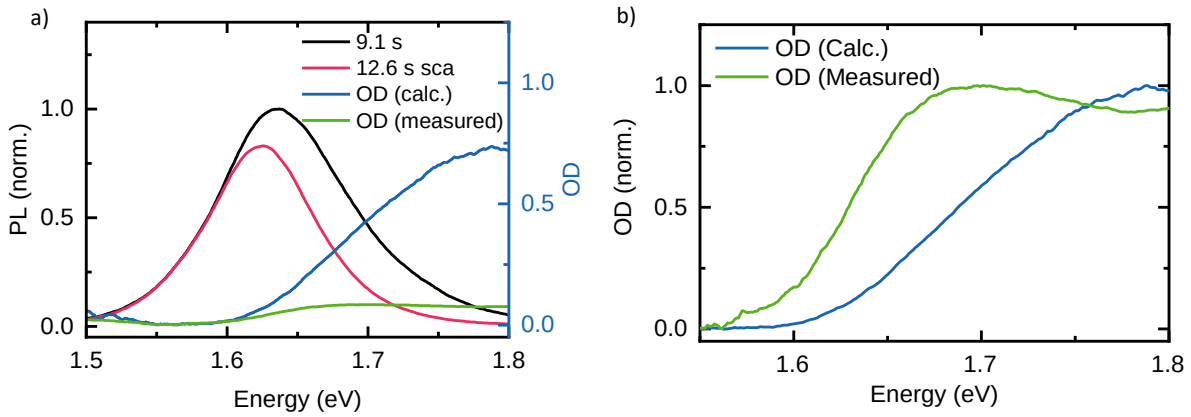

Figure S4: (a) PL at t = 12.6 s (red) scaled to the lower energy edge of the PL at t = 9.1 s (black) together with the calculated optical density if the spectral change was due to self-absorption (blue line) and the measured absorption edges determined by the measured optical density (green) at t = 12.6 s, (b) Normalized calculated (blue) and measured (green) optical density at t = 12.6 s, from which the deviations in both shape and energetic position become clear.

S5: Effect of self-absorption in range III

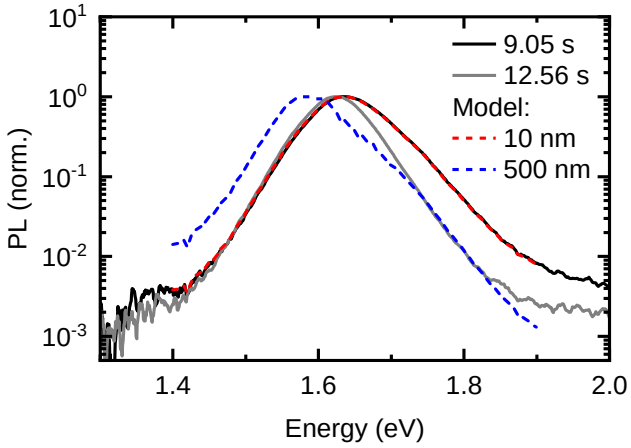

Figure S5: Normalized measured PL at t = 9.1 s (black) and t = 12.6 s (grey), together with modeled PL considering self-absorption and internal reflections, assuming the PL at t = 9.1 s to correspond to the intrinsic Pl spectrum. The significant mismatch between the modeled PL and the experimental one at 12.6 s demonstrates that the observed spectral change are not due to self-absorption effects.

S6: Difference PL spectra in range III

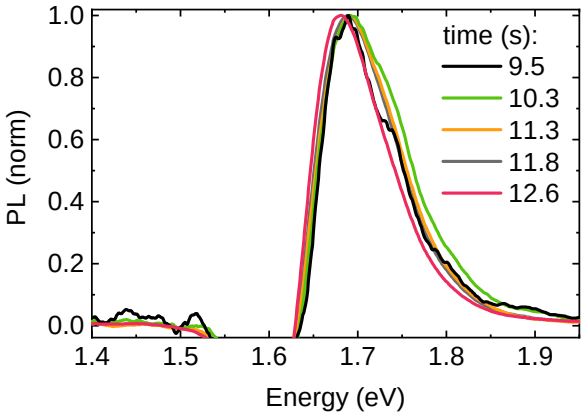

Figure S6: Normalized difference spectra between the PL spectrum at 9.1 s and the later spectra (times as indicated) in range III.

S7: Thickness Calculation from Absorption Interference at range III

Interference fringes in the measured absorption spectra were observed at the end of range III, as shown in Figure S7a t_2 = 11.6 s (red curve). Based on the appearance of this interference fringes, we can estimate the thickness of the sample, from the following equation:[2, 3]

$$d = \frac{\lambda_1 \lambda_2}{2(\lambda_1 n_2 - \lambda_2 n_1)} \quad \text{(S1)}$$

d: thickness of the sample;

λ_1 and λ_2: the wavelength at two adjacent maximum or minimum intensity;

n_1 and n_2: the sample refractive index at λ_1 and λ_2.

To quantify the value of λ_1 and λ_2, we use the normalized absorption e.g. at t_2 = 11.6 s and subtract the absorption spectrum at t_1 = 9.1 s (without interference) and obtain the blue curve in Figure S7a. The refractive index has been taken from Leguy et al., Sani et al. and Riccardo et al. for $CH_3NH_3PbI_3$, isopropanol and PbI_2 respectively.[4-6] In the range between 550 – 750nm, the refractive indexes of these three materials are, 2.4~2.5 ($CH_3NH_3PbI_3$), 1.3~1.4 (isopropanol) and 3.1~3.2 (PbI_2). Depending on the chosen parameters the calculated thicknesses from Equation S1 differ (Figure S7b)

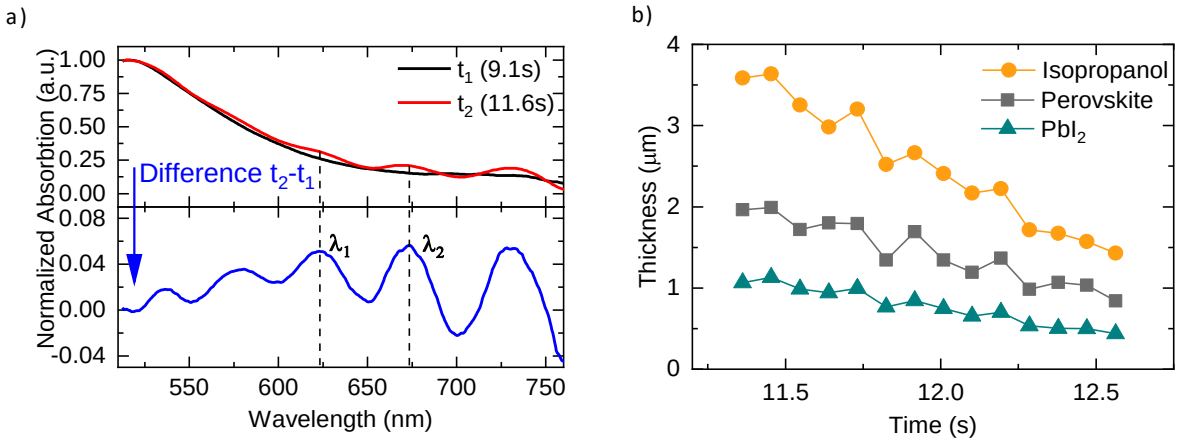

Figure S7: (a) Normalized absorption spectra at 9.1 s (black) and 11.6 s (red). The blue curve indicates the difference of absorption at t_2 and its original absorption at t_1 and was used to extract λ_1 and λ_2 (b) The calculated thickness from the interference fringes using the refractive index of isopropanol (yellow dots), $MAPbI_3$ (grey squares) and PbI_2 (green triangles).

S8: Estimation of $MAPbI_3$ thickness from absorption data

From Lambert-Beer law,

$$I = I_0 e^{-a*d} \quad \text{(S2)}$$

I_0: Incident intensity;

I: Transmittance intensity;

a: Absorption coefficient;

d: Film thickness.

Then we can obtain the thickness from the following equation:

$$a = 2.303\ (\frac{OD}{d}) \quad \text{(S3)}$$

OD: Optical density.

The absorption coefficient is extracted from literature,[7] as illustrated in Figure S8a. Figure S8b shows comparison of experimental absorption spectra and calculated absorption with thickness and absorption coefficient plotted in Figure 4 in the main text.

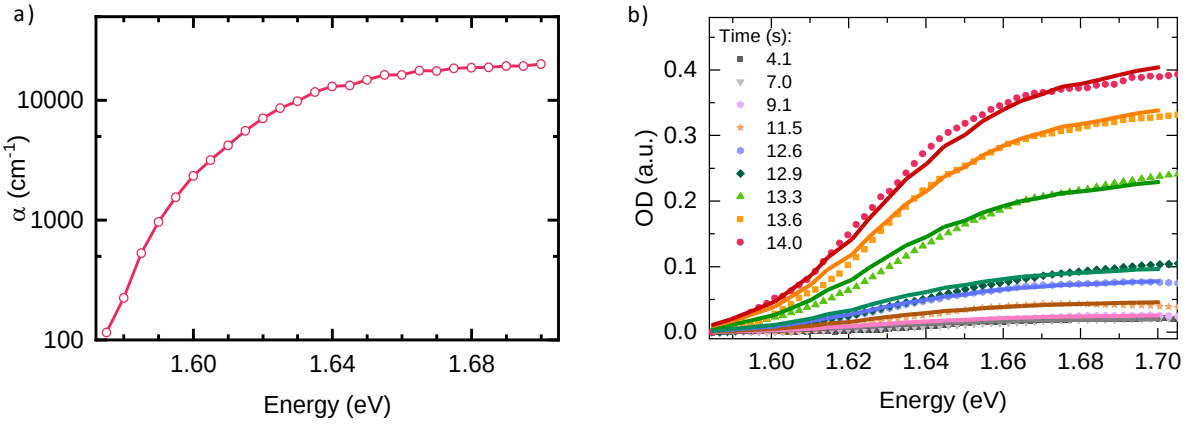

Figure S8: (a) Absorption coefficient of perovskite film used for thickness calculation,[7] (b) Experimental absorption spectra at different time (Symbol) and the corresponding calculated spectrum from absorption coefficient and thickness (lines).

S9: Calculation of growth rate in range IV

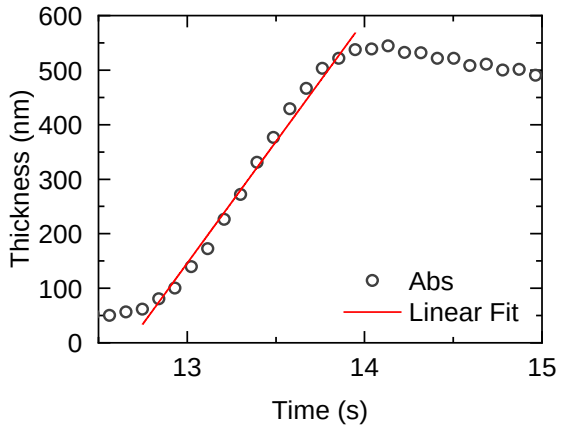

Figure S9: Linear fit to $MAPbI_3$ layer thickness in range IV to estimate the $MAPbI_3$ growth rate from resulting slope, where we find a value in the range of 445±15 nm/s.

S10: Estimation of $MAPbI_3$ thickness from the PL spectra in range IV

As outlined in our previous work,[8] for a given intrinsic PL, the detectable PL after internal reflections and self-absorption can be expressed as

$$PL_{detected}(E) = C \cdot PL_{direct}(E) + PL_{filtered}(E) \quad \text{(S4)}$$

$PL_{direct}(E)$ and $PL_{filtered}(E)$ can be calculated according to the Beer-Lambert law,

$$PL_{direct}(E) = \int_0^L PL_{int}(E) \cdot n(x)^2 \cdot \left(1 - r_f\right) \cdot exp[-\alpha(E) \cdot x]\, dx \quad \text{(S5)}$$

$$PL_{filtered}(E) = \int_0^L \sum_{j=1} PL_{int}(E) \cdot n(x)^2 \cdot \left(1 - r_f\right) \cdot \{A_j + B_j\}\, dx \quad \text{(S6)}$$

with $A_j = r_f^j \cdot r_b^j \cdot exp[-\alpha(E) \cdot (2jL + x)]$ considering the part of the PL that propagates from the site of generation, x_i , towards the front surface, and propagation towards the back surface is considered by $B_j = r_f^{j-1} \cdot r_b^j \cdot exp[-\alpha(E) \cdot ((2j-1) \cdot L + (L - x))]$. Here, $\alpha(E)$ denotes the absorption coefficient of the material, r_f and r_b are the reflection probabilities at the front and back interface, respectively, $n(x)$ is the charge carrier density and L denotes the layer

thickness. C is a suppression constant, which accounts for a mismatch of excitation and detection spot, where $C = 1$ means no suppression and $C = 0$ full suppression of the direct PL.

As the PL at the beginning of range IV is already affected by self-absorption, the intrinsic PL must be extracted by solving Equations S4-S6 for the intrinsic PL, $PL_{int}(E)$, which yields

$$PL_{int}(E) = PL_{detected}(E) \cdot \left\{ C \cdot \int_0^L \left[n(x)^2 \cdot (1 - r_f) \cdot exp[-\alpha(E) \cdot x] + \sum_{j=1} n(x)^2 \cdot (1 - r_f) \cdot \{A_j + B_j\} \right] dx \right\}^{-1} \quad \text{(S7)}$$

with L being the thickness of the $MAPbI_3$ layer at the beginning of region IV, as determined by the absorption data. The calculated intrinsic PL is shown in Figure S10. Using this intrinsic PL, the thickness of the $MAPbI_3$ layer at any time is obtained by a least-squares-fit of Equation S4, normalized, to the normalized experimental PL spectra, for a given parameter set with L being optimized.

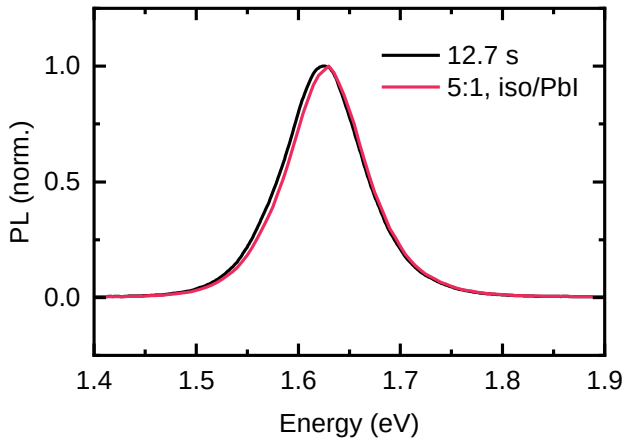

Figure S10: PL at 12.7 s and calculated intrinsic PL for an assumed layer thickness of 50 nm by inversely applying our model for calculating PL affected by self-absorption and internal reflections. The calculated intrinsic PL is then used for the estimation of the layer thickness for the following time steps.

$n(x)$ is approximated identical to the charge carrier density after laser excitation. By this, the model neglects charge carrier diffusion. In the case of thin layers, where the optical path length of the internally reflected light is on a similar length scale as the diffusion length of charge carriers, this is likely to affect the quantitative results of our model.

The reflection probabilities at the interfaces were estimated by calculating the angle-dependent reflection coefficients according to the Fresnel equations and then averaged over all possible incident angles. With refractive indices in the relevant energy range of 2.5 for $MAPbI_3$[4, 9], about 1.45 for glass[10], 1.38 for isopropanol[5], about 2.5 for PbI_2[6] and 1 for air, one obtains reflection probabilities of 0.85 for the interface $MAPbI_3$-air, 0.7 for $MAPbI_3$-glass, 0.71 for $MAPbI_3$-isopropanol and about 0 for $MAPbI_3$-PbI_2. Except for the case of $MAPbI_3$-PbI_2, reflections at other interfaces are neglected for simplicity, but would lead to an increase of the overall "effective" reflection probability. Since $MAPbI_3$ and PbI_2 are nearly index-matched, we consider instead the PbI_2-glass interface with the same reflection probability as the $MAPbI_3$-glass interface.

Figure S11a shows the obtained thicknesses for different interfaces (glass-perovskite-air (g-a) and glass-(PbI_2-) perovskite-isopropanol (g-i)) and suppression constants C, together with the one obtained from the absorption measurements. All thicknesses obtained from the modelling agree well with the ones obtained from absorption. Best agreement is obtained for PbI_2 and isopropanol as surrounding media and a suppression constant of 0.3 (g-i, 0.3; blue triangles), while all other parameter sets yield slightly lower thicknesses. However, comparing the resulting modelled PL spectra (Figure S11c-f) with the experimental ones (Figure S11b) reveals that the PL from (g-i, 0.3) (Figure S11e) agrees worst with the experimental data, especially considering the temporal evolution of the high energy falling edge. Second best agreement considering the thicknesses is obtained with (g-i, 0.2), where also the modelled PL spectra (Figure S11f) match the experimental ones nicely. A very similar result is obtained with (g-a, 0.3), and (g-a, 0.2) yields again slightly smaller thicknesses.

To capture the temporal evolution of the thickness more accurately by our model, it would probably be necessary to consider a transition of the interfaces, starting from PbI_2 and isopropanol and ending with glass and air as surrounding media. Since we have no indication on when and how this transition happens, we can not examine this scenario closer.

However, we want to stress that even with the simple model discussed above, good agreement between the thickness from the PL modelling and the one from absorption measurements could be obtained. Further, this clearly demonstrates that the observed red-shift of the PL in range IV is due to self-absorption, and represents a good example of the magnitude of self-absorption, despite excitation and detection being on the same side of the thin film.

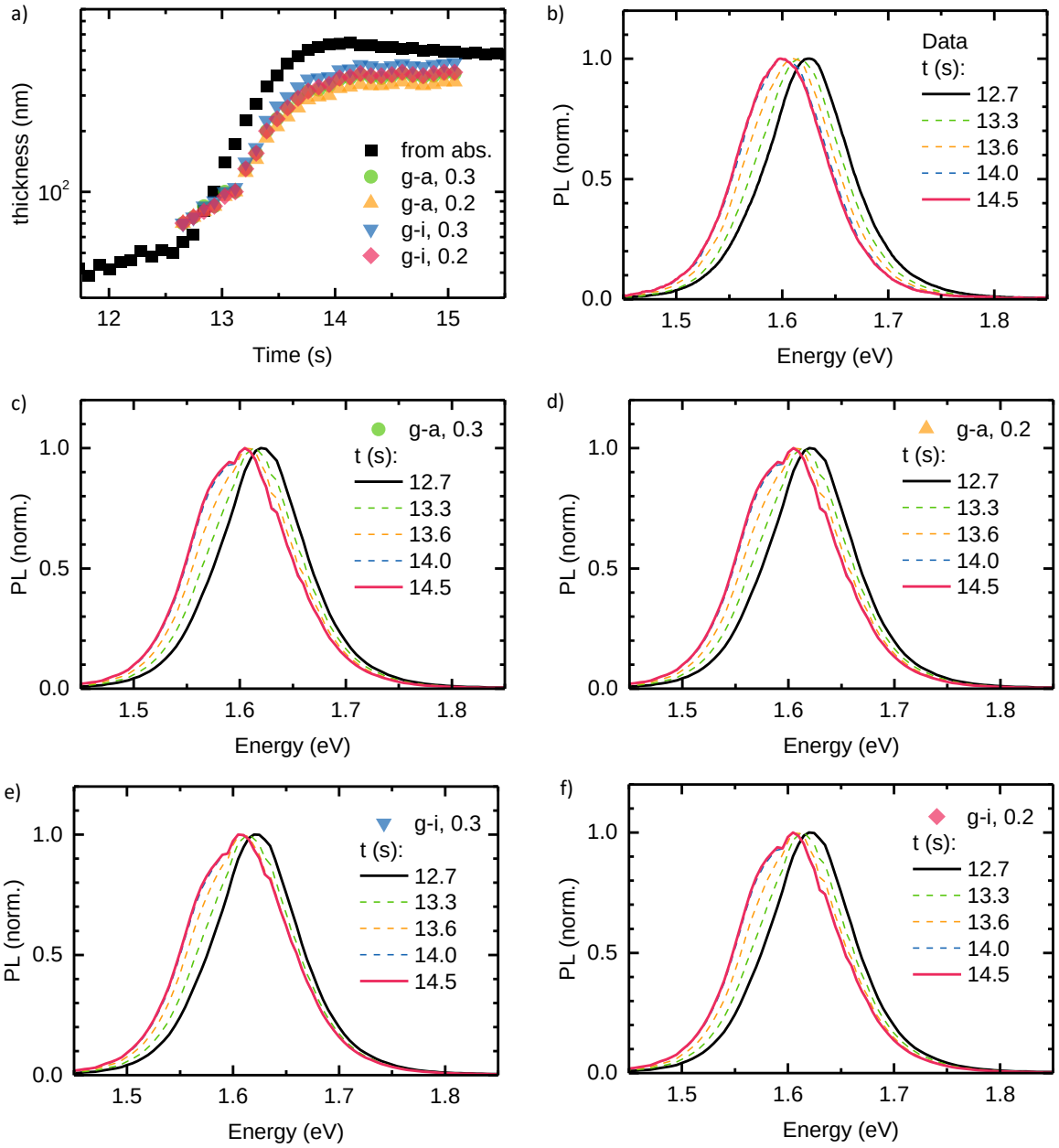

Figure S11: (a) $MAPbI_3$ layer thickness obtained from absorption measurements (black squares) together with the ones from optical modelling considering internal reflections and self-absorption. (b) Experimental PL spectra in range IV. (c-f) Modelled PL spectra considering internal reflections

and self-absorption for different surrounding media (that is glass and air (g-a), or glass and isopropanol (g-i)) and different suppression constants of 0.3 and 0.2.

S11: XRD measurements of the sample

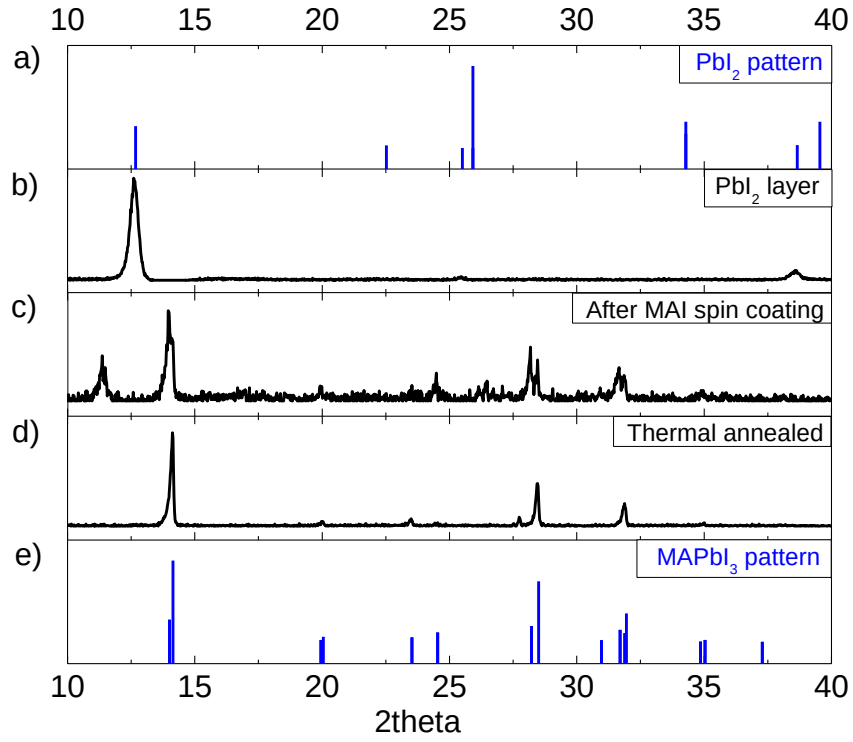

Figure S12: XRD pattern of (a) PbI_2 and (e) $MAPbI_3$ obtained from references.[11, 12] XRD spectra of (b) PbI_2 layer on glass substrate, (c) with MAI solvent spin coated on the PbI_2 layer and (d) the MAI + PbI_2 film after 45min thermal annealing.

Figure S12c shows that the formation of perovskite after the spin coating of MAI solvent. The peak 2theta = 11.4° suggests the existence of dihydrate $(MA)_4PbI_6{\cdot}2H_2O$.[4, 13] while any sign of remaining educt phase e.g. PbI_2 is absent. After thermal annealing, the signal from the dihydrate completely vanishes (Figure S12d).

S12: Estimation of average grain size of $MAPbI_3$ from SEM and theoretical model

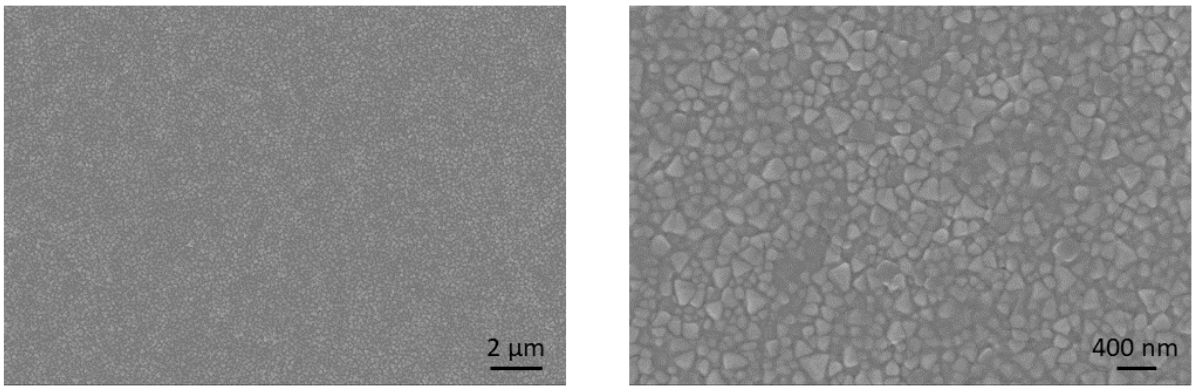

Figure S13: SEM images of the prepared film after spin coating. It yields compacted perovskite crystals. The size of the grains is between 50 nm-300 nm.

Theoretical model:

Ahn et al. derived the interaction formula to correlate grain size (Y) with MAI concentration (X) used in two step processing given as:[14]

$$\ln Y = \frac{1.22}{(\ln X - \ln C)^2} + 3.73 \quad \text{(S8)}$$

Here, C = 0.02 M MAI solution has been taken as equilibrium concentration by assuming that 0.02 M MAI solution could not react with PbI_2 films at room temperature. Using these conditions, grain size expressed as:

$$Y = exp(1.22/((\ln(X) - \ln(0.02))^2) + 3.73) \quad \text{(S9)}$$

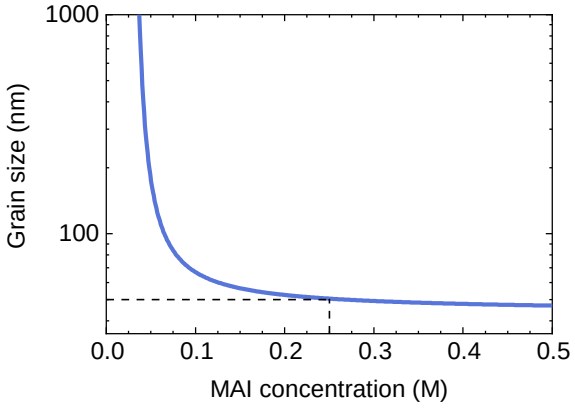

Figure S14: Average grain size of $MAPbI_3$ as a function of MAI concentration based on the model presented by Ahn et al.[14] The calculated grain size for 0.25 M (40 mg/ml) concentration (used for this study) is about 50 nm.

S13: Estimation of local heating due to laser excitation

The temperature change of the excitation spot during laser light illumination is generally determined by the heat delivered Q, divided by the heat capacity C of the material, thus $\Delta T = Q/C$. The delivered heat by the laser per time $\frac{\Delta Q_{Laser}}{\Delta t}$ is proportional to the laser fluence E_e multiplied by the area of the excitation spot A_{spot}. However, one has to consider that not all the laser light is absorbed. For the excitation wavelength of 520 nm, we observed a maximal optical density of 1 for the perovskite samples, thus 90 % of the laser light is absorbed, neglecting reflection, which would reduce the amount of absorbed light further. Additionally, not all of the absorbed energy is transformed into heat. One part of heat is provided by thermal relaxation of the carriers from their initial energy to the energy of the band gap, which gives a fraction of $\frac{\Delta E}{E_{photon}} = \frac{2.38\ eV - 1.63\ eV}{2.38\ eV} = 0.315$. The relaxed charge carriers can then either recombine radiatively or non-radiatively, producing heat. Assuming a PLQY of 0.1, corresponds to a fraction of non-radiative decay of 90%, so that we get another fraction of $\frac{1.63\ eV \cdot 0.9}{2.38\ eV} = 0.616$. Thus in sum, a fraction of $f = 0.931$ of the irradiated energy is transformed to heat.

Since the sample is illuminated continuously during one frame (approx. 0.045 s) and the heat is not delivered instantly, one has to consider the cooling of the heated spot by thermal transport through the substrate to the spin coater. This is given by the heat equation:

$$\frac{\Delta Q}{\Delta t} = \frac{\lambda \Delta T}{l} A \qquad \text{(S10)}$$

where λ is the thermal conductivity, ΔT is the temperature of the bath minus the temperature of the excitation spot, A is the area normal to the heat flow, and l is the length over which the dissipation takes place. Since the spot size is large compared to the thickness of the perovskite layer, lateral heat transport can be neglected and $A = A_{spot}$.

In thermal equilibrium, the decrease of heat by thermal transport is equal to the increase of heat by laser irradiation,

$$\frac{\Delta Q_{ges}}{\Delta t} = \frac{\lambda \Delta T}{l} A_{spot} + E_e \cdot f \cdot A_{spot} = 0 \qquad \text{(S11)}$$

Rearranging this equation for ΔT gives

$$-\Delta T = \frac{E_e \cdot f \cdot l}{\lambda} \qquad \text{(S12)}$$

Considering the spin coater as a thermal bath with a constant temperature of 300 K, the heat transport takes place over the thickness of the substrate, that is $l = 1\,mm$. The thermal conductivity of fused silica, which transports the heat, is $\lambda = 1.5\,\frac{W}{Km}$.[15] The fluence of the laser was determined to be $E_e = 75\ mW/cm^2$. Inserting this into equation S12, gives a heating of the sample of $|\Delta T| \approx 0.5\ K$ upon laser exposure.

References

1. E. S. Parrott, J. B. Patel, A.-A. Haghighirad, H. J. Snaith, M. B. Johnston and L. M. Herz, *Nanoscale*, 2019, **11**, 14276-14284.
2. J. Manifacier, J. Gasiot and J. Fillard, *J. Phys. E: Sci. Instrum.*, 1976, **9**, 1002.
3. R. Munir, A. D. Sheikh, M. Abdelsamie, H. Hu, L. Yu, K. Zhao, T. Kim, O. E. Tall, R. Li and D. M. Smilgies, *Adv. Mater.*, 2017, **29**, 1604113.
4. A. M. Leguy, Y. Hu, M. Campoy-Quiles, M. I. Alonso, O. J. Weber, P. Azarhoosh, M. Van Schilfgaarde, M. T. Weller, T. Bein and J. Nelson, *Chemistry of Materials*, 2015, **27**, 3397-3407.
5. E. Sani and A. Dell'Oro, *Optical Materials*, 2016, **60**, 137-141.
6. R. Frisenda, J. O. Island, J. L. Lado, E. Giovanelli, P. Gant, P. Nagler, S. Bange, J. M. Lupton, C. Schüller and A. J. Molina-Mendoza, *Nanotechnology*, 2017, **28**, 455703.
7. T. W. Crothers, R. L. Milot, J. B. Patel, E. S. Parrott, J. Schlipf, P. Müller-Buschbaum, M. B. Johnston and L. M. Herz, *Nano Lett.*, 2017, **17**, 5782-5789.
8. K. Schötz, M. A. Askar, W. Peng, D. Seeberger, P. T. Guijar, M. Thelakkat, A. Köhler, S. Huettner, M. O. Bakr and K. Shankar, 2019, submitted.
9. L. J. Phillips, A. M. Rashed, R. E. Treharne, J. Kay, P. Yates, I. Z. Mitrovic, A. Weerakkody, S. Hall and K. Durose, *Data in brief*, 2015, **5**, 926-928.
10. I. Malitson, *Josa*, 1965, **55**, 1205-1209.
11. K. Persson, *Materials Data on Te2MoWSeS (SG: 156) by Materials Project*, LBNL Materials Project; Lawrence Berkeley National Lab.(LBNL), Berkeley, CA …, 2017.
12. Y. Dang, Y. Liu, Y. Sun, D. Yuan, X. Liu, W. Lu, G. Liu, H. Xia and X. Tao, *CrystEngComm*, 2015, **17**, 665-670.
13. A. Halder, D. Choudhury, S. Ghosh, A. S. Subbiah and S. K. Sarkar, *The Journal of Physical Chemistry Letters*, 2015, **6**, 3180-3184.
14. N. Ahn, S. M. Kang, J.-W. Lee, M. Choi and N.-G. Park, *Journal of Materials Chemistry A*, 2015, **3**, 19901-19906.
15. B. H. De Jong, R. G. Beerkens, P. A. van Nijnatten and E. Le Bourhis, *Ullmann's Encyclopedia of Industrial Chemistry*, 2000.